INL/JOU-23-75232-Revision-0

Selective pseudocapacitive immobilization of REE elements on carbon based electrodes

February 2024

Eugene Tettey Engmann, Luis A Diaz Aldana, Tedd Lister, Abderrahman Atifi, Haiyan Zhao, Olena Palasyuk

Changing the World's Energy Future

INL is a U.S. Department of Energy National Laboratory operated by Battelle Energy Alliance, LLC

INL/JOU-23-75232-Revision-0

Selective pseudocapacitive immobilization of REE elements on carbon based electrodes

Eugene Tettey Engmann, Luis A Diaz Aldana, Tedd Lister, Abderrahman Atifi, Haiyan Zhao, Olena Palasyuk

February 2024

Idaho National Laboratory
Idaho Falls, Idaho 83415

http://www.inl.gov

Prepared for the
U.S. Department of Energy
Under DOE Idaho Operations Office
Contract DE-AC07-05ID14517

Selective Pseudocapacitive Immobilization of REE Elements on Carbon Based Electrodes

Eugene Engmann[1,3], Luis A. Diaz[1,*], Tedd E. Lister[1], Abderrahman Atifi[1] Olena Palasyuk[2], Haiyan Zhao[4]

[1]Critical Materials Innovation Hub, Idaho National Laboratory, 2525 Fremont Avenue, Idaho Falls, ID 83402, USA
[2]Ames National Laboratory, Department of Energy U.S., Critical Materials Innovation Hub, Ames, IA 50011-3020, US
[3]University of Idaho, Department of Nuclear Engineering and Industrial Management
[4]University of Idaho, Department of Chemical and Biological Engineering

***Corresponding Author**

Luis A. Diaz
Phone: (208) 526-7411
Email: Luis.DiazAldana@inl.gov
Fax: (208) 526-5086
P.O. Box 1625, MS 3731
Idaho Falls, ID 83415

Abstract

Current extraction technologies for rare earth elements at ambient conditions are reagent and energy intensive, giving rise to significant quantities of secondary waste streams. Exploration of the removal of common cations from aqueous streams has been undertaken with carbon materials and have shown promising results. However, those promising materials have not been explored extensively for rare earth element capture from aqueous process streams. In this study, a carbon electrode was investigated for the adsorption and immobilization of REE elements from aqueous solutions. Cyclic voltammetry studies of the carbon electrode displayed a pseudocapacitive behavior where it was verified that cation adsorption is accompanied by an electron transfer process. Preliminary tests showed that a current density of 89.1 mA. g^{-1}, allowed for the pseudocapacitive adsorption (PSA) of Nd^{3+} cation without the formation of rare earth hydroxides. Hence, the selective PSA of Nd^{3+} was verified in an electrolyte solution with equimolar concentrations of Nd^{3+}, Mg^{2+}, Li^{+}, Na^{+} and K^{+}, achieving separation factors of 8.6, 1.1, and 10.9 for Nd^{3+}/Li^{+}, Nd^{3+}/Na^{+}, and Nd^{3+}/Mg^{2+}, respectively. Analysis of the potential-time curves for the various cations suggests that storage of ions in the electrode involved pore-spacings rather than interlayer spacings and was corroborated by XRD analysis. Specific capacitance as high as >640 $F.g^{-1}$ for Nd^{3+} was also observed for the carbon electrode, with Faradaic efficiencies (FE) of > 20% for Nd^{3+} and Mg^{2+}, and > 9% for Na^{+}. Furthermore, adsorption capacity of >125 mg g^{-1} after 4hrs of electrosorption was observed for Nd^{3+}. In the presence of the Nd^{3+} electrolyte, the electrode achieved increasing storage of Nd^{3+} with >94% retention of Nd^{3+} with a FE > 20% over 6 cycles between loading and releases in 1 M KCl solution. These preliminary results provide information and some guidance on the selective recovery of rare earth elements, such as Nd, in aqueous streams in the presence of competitive cations employing the use of carbon-based materials.

Key words: Pseudocapacitive immobilization, Electrosorption, Rare earths separation

Introduction

Rare earth elements (REEs) markets have seen increased growth driven by advancement of materials and applications, such as permanent magnets, catalysts, and optical technologies [1, 2]. With this high demand of REEs, there arises the need to investigate and develop technology for the recovery and extraction of REES from nonconventional sources such as acid mine drainage [3] or coal fly ash leachates [4-6].

At present the recovery of REEs from aqueous streams have included, solvent extraction, precipitation, ion exchange filtration, as well as adsorption [7]. In the case of adsorption, adsorbents such as activated carbon, graphene oxides, and carbon nano tubes are employed due to large surface area and the presence and ability to synthesize functional groups [8, 9]. However, the drawback to chemical adsorption is the slow nature of the process and requirement of chemicals to strip adsorbed ions from the surface of the absorbents [9].

Electrosorption has gained interest in the field of REEs due to the encouraging results for capture of metal ions from wastewater streams [8, 9]. Technologies such as capacitive deionization (CDI) have shown growing interest and are being developed for the extraction of REEs from dilute streams [10]. Wang et al. employed the use of CDI for REE extraction, reporting adsorption capacities of Nd^{3+}, Ce^{3+}, and La^{3+} of approximately 600 mg g^{-1} on sodium diphenylamine sulfonate modified activated carbon after 800 minutes [9]. However, REE products were captured in the form of hydroxides $REE(OH)_3$ a

Faradaic driven processes that is electrochemically irreversible. Adsorption of $REE(OH)_3$ requires an acid to recover the REEs as ions from the substrate. Thus, adding additional steps and chemical requirements to the recovery process. Zhao et al. employed CDI at lower cell voltages to selectively capture La^{3+} from Fe^{3+}, Ca^{2+}, and Na^{+}. With a purely capacitive process, they observed an electrosorption capacity of 23.66 mg g^{-1} for an electrolysis time of 25 minutes, at optimum conditions, followed by the release of metals at open circuit potential [8].

Recently, a group of materials termed as pseudocapacitors (PCs), whose charge storage are driven by both capacitive and surface Faradaic redox reactions have gained interest in the field of REE electrosorption [11-13]. The redox nature of charge storage promote the adsorption of ions, beyond the formation of the electrochemical double layer, at faster rates [13]. Hence, the ability to electrosorb REE^{n+} (where n is typically 3) via pseudocapacitive process could open a path to electrochemical REE separations via an appropriate electrical potential.

The ability to increase the electrosorption capacity for large cations such as REEs requires not only a high surface area electrode, but the ability to access all available adsorption sites (pore and defects alike) within electrode material structure [14-16]. Of the many electrodes available to explore, graphitic carbon materials such as hard and soft carbons possess excellent traits such as high capacity, larger surface areas, and surface Faradic redox couples [11-13, 17, 18]. The electrosorption on carbon materials is fostered by the rich presence of surface functional groups such as oxygen and nitrogen containing groups [19]. Adsorption of heavy metal by functional groups occurs through the mechanisms of physical adsorption, electrostatic interaction, surface complexation and precipitation [19].

Consequently, hard and soft carbons have been explored and studied extensively for cation storage such as Li^{+} [20-22] , Na^{+} [15, 23, 24], and K^{+} [25-27], and have shown superb capacitance ranging from 200 F g^{-1} to >2000 F g^{-1} [28]. Such high capacity and fast cycling present opportunities for other beneficial applications such as REE recycling and electrosorption, as well as the concentration of cations such as Li^{+}, Na^{+}, K^{+} and Mg^{2+} from dilute aqueous streams. Furthermore, the abundance of defects, disordered planes, and surface porosity sizes make these carbon materials ideal candidates for large ion storage [29-36].

Beyond the aforementioned REEs electrosorption experimental research, no systematic mechanistic studies have been reported on the REEs electrosorption on carbon-based electrodes. On the other hand, numerous studies have been performed to elucidate the electrosorption mechanism of Na^{+} for energy storage in nonaqueous organic electrolytes [15, 33, 37, 38], which could serve as starting point to understand the behavior of REE electrosorption. While investigating the electrochemical storage of sodium in carbon materials, Cheng et al. observed two storage phenomena. Firstly, sodium was stored partially through intercalation, and secondly through defect adsorption (pore spacing) [15]. Other researchers have likewise explored this area thoroughly and have arrived at the same conclusion [33, 37, 38]. Furthermore, not only Na^{+} but Li^{+} and K^{+} among many other cations have also been studied for electrosorption into various carbon materials as energy storage applications [39-43].

This work investigates and examines the selective electrosorption of Nd^{3+} and separation from common cations (Na^{+} and Mg^{2+}) as a means of loading/unloading these metal ions via a conductive carbon electrode (Vulcan XC-72R). Li^{+}, Na^{+}, K^{+}, Mg^{2+} were selected for this study based on their presence as major elements in diluted REE streams such as coal fly ash [44]. Accordingly, the monovalent and divalent effects of counterions on Nd^{3+} separation from a mixed stream, was investigated and simulated

employing the use of Na^+, and Mg^{2+}. The application of pseudocapacitive processes is used to achieve REEs removal from an aqueous stream and release them via an applied electrical potential into a blank electrolyte.

Experimental

Electrode Preparation. —Carbon paste slurries were made from a mixture of 80 wt.% carbon powder (Vulcan XC 72R, Fuel Cell Store), 20 wt.% polyvinylidene fluoride, and N-methyl-2-pyrrolidone (NMP) as a solvent (Sigma Aldrich). The Vulcan XC 72R was used as received. The solvent to powder ratio was 2:1. Slurries were painted on 4 cm^2 carbon paper (Toray Teflon Treated Carbon Paper- 060 - TGP-H-060) substrates. The mass loading of the electrode was 32 mg carbon. Electrodes were dried at room temperature.

Electrolyte Composition. —Aqueous and ionic liquid (IL) electrolytes were employed for electrolysis. Aqueous electrolytes employed were 250 mM $NdCl_{3(aq)}$, 250 mM $LiCl_{(aq)}$, 250 mM $NaCl_{(aq)}$, 250 mM $MgCl_{2(aq)}$, and 250 mM $KCl_{(aq)}$ or 1 M $KCl_{(aq)}$ in DI water. $NdCl_3$ was purchased from Sigma Aldrich, LiCl was purchased from RICCA, KCl and NaCl were purchased from Fisher Chemical, and $MgCl_2$ was purchased from Alfa Aesar.

Electrochemical experiments. —The electrochemical experiments were conducted in a three-electrode cell with the carbon electrode as the working electrode, and Pt as auxiliary electrode (Figure S1). Potentials were measured and reported versus an Ag/AgCl (3 M NaCl) (BASi) reference electrode. A BioLogic SP-50 potentiostat controlled by EC-Lab software was used to perform electrochemical experiments. IR compensation was applied to CV curves and bulk experiments.

Cyclic voltammetry (CV) was used to examine the electrochemical window in various electrolyte systems. Galvanostatic tests were employed for loading and release of the REEs into the carbon electrode.

Analysis of electrochemical data. —The specific capacitance of the carbon electrode was calculated as shown in Equation 1:

[1]

where is the specific capacitance in $F.g^{-1}$, A is the area of the hysteresis loop or CV plot in mA.V, v is the scan rate in $mV.s^{-1}$, ΔV is the potential window in V, and m is the mass of the active material in grams.

Following electrolysis, the electrodes were rinsed with DI water and then digested in 3:1 HCl-HNO_3 (aqua regia) to determine the total amount of metals ions electrosorbed on the electrode. The expected amount of metal ion in the carbon electrode based on charge density can be calculated as

[2]

where m_i is the mass (g) of the electrosorbed ion, M_{wi} (g/mol) is the molecular weight of the electro-sorbed ion, C_h (mAh) is the electrical charge capacity of the host, n_i is the number of electrons going towards the reaction and F (C/mol) is the Faraday constant.

Analysis and Characterization Methods. —Following chronopotentiometric (CP) electrosorption of cations from their respective electrolytes, the carbon electrodes were washed with copious amounts of DI water, dried, and introduced to 1 M $KCl_{(aq)}$ to release metal ions. After electrochemical release, the

electrodes were digested in aqua regia to quantify the remaining metal ions in the electrode. The concentration of metal ions released in the KCl as well as the HCl-HNO_3 leachate was measured using an iCAP Q inductively coupled plasma mass spectrometer (ICP-MS) from Thermo Scientific. SEM and EDS analysis were employed to study elemental composition, and surface morphology. A JEOL JSM-6610LV and EDAX AMETEK Apollo X controlled by EDAX software was employed for SEM and EDS studies. FIB analysis was employed to investigate the subsurface of the carbon electrode. XRD analysis was conducted to investigate structural makeup and possible changes to the carbon electrode prior to, and after REE electrosorption using a Bruker D8 Advance Diffraction System (Cu Kα radiation, λ = 1.54056 Å) with a Bragg-Brentano geometry, operated at 40 kV and 40 mA with the following parameters: 2θ region 10–90˚; step scan 0.02˚; counting time per step 60s. Based on the XRD spectra, structural properties of Vulcan-XC-72R was elucidated using the Scherrer [45], Warren-Scherrer [46], and Braggs law equations [47, 48] (See Supplementary information)

Results and Discussions

Characterization and Controls Prior to Electrosorption

The morphology and elemental composition of the as prepared electrode was explored employing SEM and EDS prior to electrosorption. Figure 1a, b, c shows an even coating of the active material with a smooth and porous morphology. Furthermore, Figure 1c shows incorporation of the active material into the fibers of the carbon paper substrate, suggesting strong adhesion to the carbon paper substrate. Thus, contributing to the mechanical stability of the active material. EDS analysis of the active material in Figure 1 d and e, shows a strong presence of carbon. Other elements present are contributions from the binder. Furthermore, traces for Nd in the blank electrode were investigated and suggest a very weak presence (trace quantities) of Nd^{3+} in the electrode. This is corroborated by ICP-MS analysis of an aqua regia analyte in which the "as prepared" electrode was digested, and Nd^{3+} present was 3.06 $X10^{-6}$ mg g^{-1} for Nd. While this value is very insignificant, it cannot be ignored because the ICP-MS used in this study can detect Nd^{3+} to the parts per trillion with a 94% recovery rate.

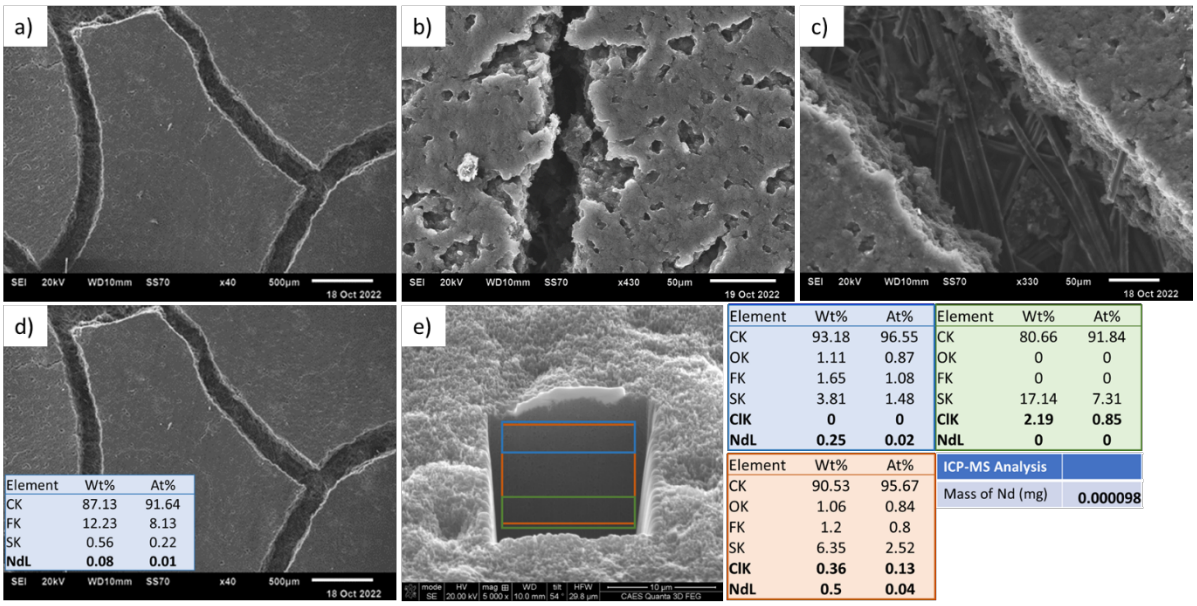

Figure 1. a)-c) SEM of the blank carbon electrode, d) and e) EDS analysis of the surface and subsurface of the blank carbon electrode respectively.

Electroless Adsorption of Nd^{3+} — A baseline test was performed to validate the Faradaic electrosorption of Nd^{3+} into the carbon electrode. To establish the baseline, a 4 cm^2 electrode with a carbon loading of 32 mg (8 $mg.cm^{-2}$) was immersed overnight in 250 mM $NdCl_{3\,(aq)}$ at open circuit potential (OCP). Following immersion, the electrode was rinsed thoroughly with DI water, analyzed with EDS and digested in aqua regia for further characterization. EDS analysis as shown in Figure S2 shows a negligible amount of Nd present on the electrode. ICP-MS analysis of the leachate revealed that the total amount of Nd^{3+} present in the electrode was 0.00254 mg g^{-1}. Factors resulting in this value could be contributions from chemisorption or residue of Nd^{3+} from the electrolyte following thorough washing.

Cyclic Voltammetry (CV) of Carbon Electrode in Aqueous Li, K, Na, Mg, and Nd Electrolyte —The CV sweeps for the carbon electrode in $NdCl_3$ solution (Figures 2a and S3) illustrates broad and less prominent peaks as well as well as features typical of a pseudocapacitive material. These patterns are characteristic potential current responses for pseudocapacitors, where no prominent redox peaks are observed [57]. Only a broad reduction peak is observed between 0.5 and -1 V vs Ag/AgCl, and a broad oxidation peak near 0.5 V vs Ag/AgCl.

The presence of the broad reduction peak during the CV sweeps suggests slow diffusion of species into the carbon electrode [11, 17, 28] . Furthermore, the prompt increase in current density upon voltage reversal at cathodic and anodic switching potentials suggest expeditious electrosorption and desorption of the various metal ions, respectively, at the surface of the electrode [49, 50]. These observations are in agreement with the proposed cation storage mechanisms of pseudocapacitors where charge is stored through a possible combination of surface redox pseudocapacitance, and intercalation pseudocapacitance [12, 13, 51].

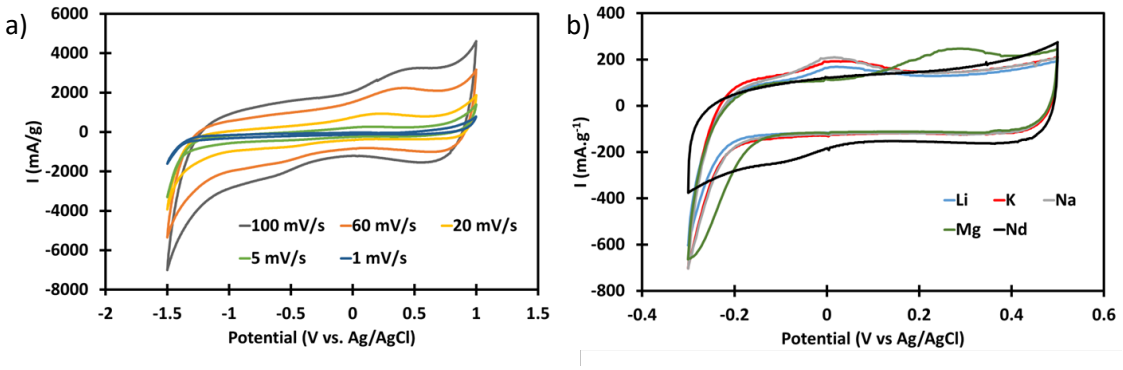

Figure 2. Cyclic voltammetry of an 8 $mg.cm^{-2}$ carbon (Vulcan XC-72R) electrode in 250 mM aqueous a) $NdCl_{3(aq)}$ electrolyte at various scan rates of 1 mV/s to 100 mV/s within a potential window of -1.5 V to 1.0 V vs Ag/AgCl. b) CV of various elements at 20 mVs^{-1} showing positive electrosorption peak for Nd^{3+} within a potential window of -0.3 V to 0.5 V vs Ag/AgCl.

Figure 2b shows a comparison of the CVs obtained at 20 mV/s for the carbon electrodes in solutions containing different metal cations representing tri, di, and monovalent states (Nd, Li, Mg, Na, and K). Figure 2b further shows that in the pure capacitive region of -0.3 V to 0.5V vs Ag/AgCl, a more positive broad peak displayed at -0.1 V vs. Ag/AgCl for the Nd system could be attributed to the electrosorption of Nd^{3+}. Thus, suggesting a possible selectivity for Nd^{3+} electrosorption over the other cations at more positive potentials. CVs at different scan rates within this same potential window, for all tested ions, are

displayed in Figure S4 and show that no peak ca. -0.1 V vs. Ag/AgCl is observed in the absence of Nd^{3+}.

Furthermore, Figures S3f, shows that for an electrolyte containing equal concentrations of Nd^{3+}, Mg^{2+}, Li^{+}, Na^{+}, K^{+}, the CV plot displays identical features as that of an electrolyte containing only Nd^{3+}, suggesting possible favorability of Nd^{3+} in a mixed stream.

Specific Capacity (SC) of Carbon Electrode in Aqueous Li, K, Na, Mg, and Nd Electrolyte —The SC of the electrodes in the various electrolytes was calculated based on the CVs in Figure S3. Figure 3 and Table S1 show that as the scan rate decreases, the SC of the carbon electrode increases. This suggests that for fixed potential adsorption, longer electrolysis duration results in substantial capture of cations. Furthermore, the carbon electrode demonstrated the highest SC of 1037 $F.g^{-1}$ in the presence of Li^{+}, and 584, 861, 336, and 646 for K^{+}, Na^{+}, Mg^{+}, and Nd^{3+}, respectively, as seen in Figure 3. Compared to literature [52], these capacity values are higher, than those reported for Vulcan XC 72R and Vulcan XC 72 in various electrolytes [52-54]. Furthermore, they are comparable to SC values reported for graphite compounds in the presence of these cations [28].

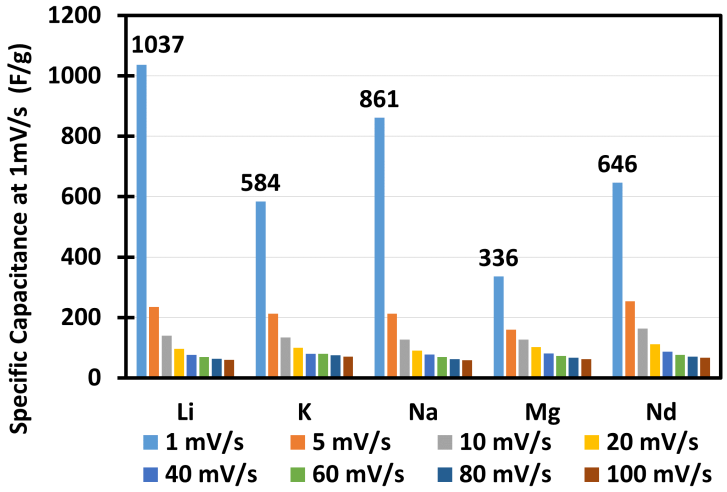

Figure 3. Specific capacity of 8 $mg.cm^{-2}$ carbon electrode in 250 mM aqueous $LiCl_{(aq)}$, $NaCl_{(aq)}$, $KCl_{(aq)}$, $MgCl_{2(aq)}$ and $NdCl_{3(aq)}$ electrolyte at various scan rates.

Investigating Storage Capacity of the Carbon Electrode for Nd^{3+} Electrosorption —Efficient electrosorption of Nd^{3+} on the carbon electrode requires an understanding of the storage capacity of the carbon electrode in the presence of Nd^{3+}. While this is not known for Vulcan XC-72R, a careful stepwise approach can be employed to get an idea of this value. From the CV scans at different scan rates, it was observed that the slowest scan rate yielded the highest specific capacitance (Figure 3). Likewise, a much smaller current density application will yield a storage capacity closer to the true value of the electrode for a given applied charge [63, 64]. To investigate this, a cathodic current density of -18.75 mA g^{-1} was chosen to electrosorb Nd^{3+} over a 24-hour period. The electrolyte was 1 M $NdCl_3$. The cutoff potential or

negative limit was 0 V vs Ag/AgCl. After approximately 19 hours of electrolysis the experiment reached the cutoff potential with corresponding storage capacity of 11.41 mAh or 356.9 mAh.g^{-1} and a charge density of 1284 C g^{-1} as seen in Figure S5. These values correspond to a theoretical value of 20.5 mg of Nd, from Equation 2, assuming a Faradaic efficiency (FE) of 100%. Based on this value, the effect of operating current and time can be investigated to optimize Nd^{3+} electrosorption. For practical application, a shorter run time at an applied current density that does not compromise the future electrode function is desired.

Effect of Current Density on Nd^3 Electrosorption —Applied current densities have a significant influence on processes happening on the electrode surface when mass transfer limitations are present. 2-, 4- and 6-hour experiments were performed to study the effect of current density on Nd^{3+} electrosorption based on the charge density of 1284 C g^{-1}. These durations corresponded to applied current densities of 178 mA. g^{-1}, 89.1 mA. g^{-1}, and 59.4 mA. g^{-1}, respectively. Experiments were performed using 11 mL of 250 mM $NdCl_{3(aq)}$. Figure 4a shows the time vs. potential curves for these experiments. After a rapid initial decrease in potential these curves plateau at voltages which are lower for the shorter (higher current) experiments.

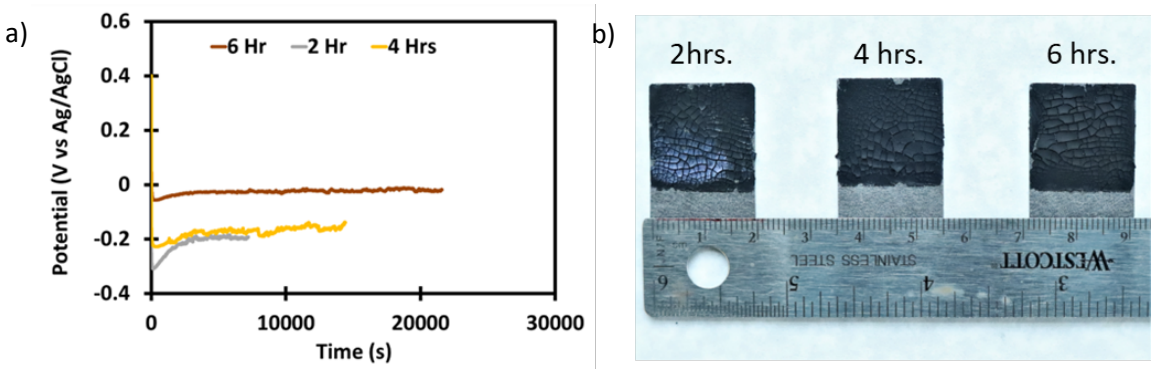

Figure 4. a) Time vs. potential curve for 2-, 4- and 6-hour experiments. b) Photographs of electrodes at 2 hours of electrolysis at 178 mA. g^{-1} showing visible precipitate, and 4 and 6 hours of electrolysis at 89.1 mA. g^{-1} and 59.4 mA. g^{-1} respectively with visual absence of pastel precipitate on electrode.

In studying the electrosorption of Na^+ on hard carbon in organic based nonaqueous electrolytes, researchers have attributed the sloping region of the time vs. potential curve to the intercalation of Na^+ between the layers of the carbon electrode [15, 34]. They further attribute the plateau region to the adsorption of Na^+ within defects such as pores [15, 34]. In an experiment, Bai et al. prefilled the pores of the carbon electrode with sulfur via vapor infusion methods prior to Na^+ electrosorption, and observed the disappearance of the plateau region and the lack of Na^+ incorporation [38]. These observations along with the results presented by other studies [32, 33, 55, 56], and the shape of the Nd^{3+} electrosorption potential profiles (Figure 4) can be used to hypothesize that the mechanisms associated with Nd^{3+} storage, as well as for other cations employed in this study, occur within the pores of the carbon electrode similar to that described for Na^+ electrosorption.

Following electrosorption, the visual inspection of the electrode surface displayed a pastel purple precipitate on the electrode polarized for 2 hours as seen in Figure 4b. No visible precipitates were observed for the electrodes polarized for 4 and 6 hours. While the potential time curves of 4 hours and 2 hours are similar, a more negative current density could promote the hydrogen evolution reaction (HER) at the surface of the electrode leading to the formation of $Nd(OH)_3$. A similar observation was

made by Medina et al, where HER at the surface of the cathode was used to concentrate La^{3+} from solution in the form of $La(OH)_3$ [57]. EDS analysis of the various electrodes as seen in Table 1 and visually represented in Figure S6 show that the ratio of oxygen to Nd for the 2-hour electrode strongly supports the formation of $Nd(OH)_3$ surface precipitates; which is not a desired product for this study. Low oxygen to Nd (O:Nd) ratios are obtained for both 4 and 6 hours tests. However, lower chloride to Nd (Cl:Nd) and (C:Nd) ratios obtained for the 4 hr experiments over the 6 hr test suggest that shorter times (higher currents) could favor the adsorption of Nd over counter ions [58, 59].

Table 1. Various elemental ratios to Nd^{3+} of EDS measurements. 2, 4, 6 hours of electrolysis corresponding to 178 $mA.g^{-1}$, 89.1 $mA.g^{-1}$, and 59.4 $mA.g^{-1}$ respectively. The electrolyte was 250 mM $NdCl^{3+}$ and the electrode was 8 $g.cm^2$.

Time (Hr.)	O:Nd	C:Nd	Cl:Nd
2	3.81	34	0.506
4	1.22	64	0.420
6	1.8	100	0.482

ICP-MS analysis of the various analytes obtained after Nd^{3+} electrosorption at 2, 4 and 6 hours shown in Table 2 show an average Nd^{3+} loading of 7.3, 4.6, and 3.5 mg, respectively. FE, calculated based on an expected 20.5 mg theoretical value (Equation 2), decreased from an average of 35.7% to 22.5% to 16.9% for 2, 4, 6 hours respectively. It should also be noted that at 2 hours, the formation of $Nd(OH)_3$ probably accounts for a significant portion of the FE value (~40%). These results suggest that higher current operations, but below the polarization limits to promote HER are desirable to enhance the electrosorption of Nd.

Table 2. Parameters for electrolysis and ICP-MS measurements of Nd^{3+} in carbon electrode following electrolysis.

Time (Hr)	Applied Current Density ($mA\ g^{-1}$)	Mass of Carbon (mg)	Charge per mg of Carbon C	Charge Per cm^2 (C)	ICP-MS of Nd in Carbon (mg)	Standard Deviation	Faradaic Efficiency	Carbon: Nd
2	-178	32.0	1.28	10.3	7.02	0.277	34.3	4.6
2	-178	32.0	1.28	10.3	7.58		37.0	4.2
4	-89.1	32.0	1.28	10.3	4.88	0.263	23.8	6.6
4	-89.1	32.0	1.28	10.3	4.35		21.2	7.4
6	-59.4	32.0	1.28	10.3	3.61	0.144	17.6	8.9
6	-59.4	32.0	1.28	10.3	3.32		16.2	9.6

Observation of an adequate current density (89.1 mA. g^{-1}) prompted investigation into the effect of electrosorption time on Nd electrosorbed, and FE. Five different 8 $mg.cm^{-2}$ electrodes were employed for this study. The data in Figure 5a suggests a linear relationship for Nd^{3+} electrosorption over time. These values agree with Equation 2 where an increase in charge density is proportionally related to an increase in the amount of Nd^{3+} electrosorbed. However, Figure 5b shows a decrease in the FE from 5 minutes to 1 hour. The FE then stabilizes around an average value of 21.9% at 2 hrs., 4 hrs., and 8 hrs. respectively. Unlike organic electrolytes where only the metal of interest is electrosorbed, in aqueous solutions, competing proton co-electrosorption is possible and cannot be ignored [60]. This due to the mobility of protons in aqueous solutions being about 4.6 times faster than other cations [58, 59, 61]. It is also known that parasitic co-electrosorption of protons suppresses the FE of charge storage electrodes

in aqueous electrolytes and affects the long-term electrochemical performance. Suggesting that the high values of FE at 5 minutes and 1 hour, implies insufficient time for proton co-electrosorption to dominate. However, as the duration of electrolysis increases, proton co-electrosorption is dominant. Nevertheless, it is promising to see that at durations of 2hrs., 4hrs. and 6 hrs., the FE stabilizes. Suggesting a saturation threshold for proton electrosorption, and a window where bulk experiments can be designed to yield satisfactory values of Nd^{3+} immobilization. Furthermore, while proton co-electrosorption suppresses FE, it has been shown to aid in extended cycle life of charge storage electrodes [62], and can be regulated based on the pH composition of the electrolyte [63].

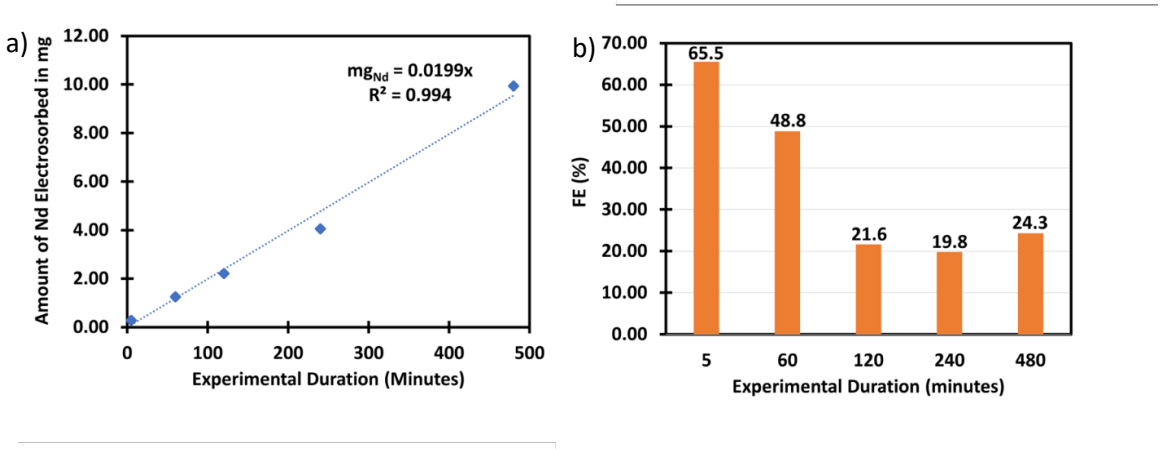

Figure 5. a) Amount of Nd electrosorbed showing a linear trend and b) Faradaic Efficiency at various duration of electrolysis in a 250 $mM_{(aq)}$ electrolyte of $NdCl_{3(aq)}$. The current density applied was 89.1 mA g^{-1}.

XRD Analysis of Vulcan XC-72R Following Electrolysis in $NdCl_3$—Information on the structural and chemical changes on the electrode following electrolysis of 4 and 14.5 hours was obtained through XRD to clearly distinguish the effects of Nd^{3+} electrosorption performed at a specific current density of -89.1 mA g^{-1} in 250 mM $NdCl_3$. XRD information was collected over the range of 15 to 80 2-θ degrees as seen in Figure 6. It should be noted that the XRD spectra in Figure 6 have been offset for clarity. Superimposed plots can be found in Figure S7.

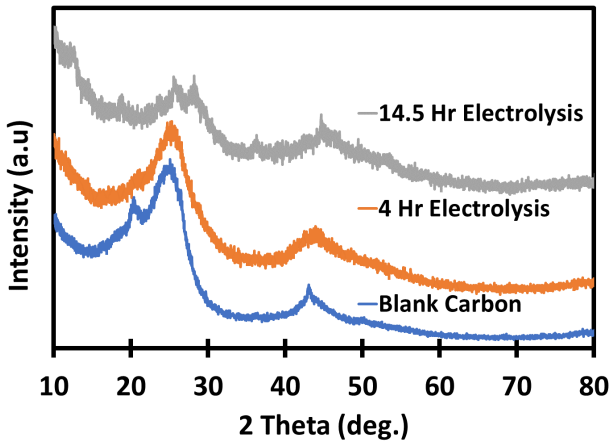

Figure 6. XRD of, blank carbon (blue trace), electrolysis after 4 (orange trace) and 14.5 hours (gray trace). XRD spectra offset for clarity.

For all samples, Figure 6 shows the classic graphite peak at 25.3° corresponding to the (002) family of planes [46]. The broadness of this peak indicates the presence of irregular amorphous disordered structures [64, 65]. Results from XRD also show a dramatic structural change within the carbon electrode at 14.5 hours. This suggests the graphite structure was highly modified with shortened length between the carbon layers [15, 66]. Furthermore, no visible peak shift of the (002) plane is observed. This suggests that the diffusion of Nd^{3+} between carbon layers is nonexistent or contributes minimally to the electrosorption of Nd^{3+} [15, 33, 37].

Also observed at 43° is a low intensity broad peak corresponding to planes of sp^2 hybridized carbon related to the family planes of (100) and (110) [67]. As the duration of electrolysis increases, these planes experience a shift to higher 2-θ angles and associated peaks broaden from a sharp apex. In this research such an observation could suggest the possibility of Nd^{3+} ions between the pores of the carbon electrode as observed by Alcorn et al. in the presence of Li [68]. Along with the XRD spectra, structural properties of Vulcan-XC-72R was elucidated in Table S2 employing the use of the Scherrer [45], Warren-Scherrer [46], and Braggs law equations [47, 48]. Furthermore, extensive research investigating the physical characteristics of Vulcan XC-72R, reported by other researchers, reveals a specific surface area, of 223-241 m^2/g, and total pore volume of 0.38-1.04 cm^3/g for the Vulcan XC 72R material. Concurrently, the average pore diameter for Vulcan XC 72R has also been reported as 10.4-18.7 nm [52, 69, 70]. With a reported hydration number of ca. 8.91 Å for Nd^{3+} in chloride solutions [71], accessibility of Nd^{3+} to pore spacing is highly probable. Thus, suggesting that the storage of Nd^{3+} in pore spacing cannot be ignored. Results from these findings strongly suggest the electrosorption of Nd^{3+} within the pore spaces of the electrode. Refer to supplementary document for detailed findings.

Electroless Release of Nd — To further study the nature of the electrosorption process, the release of Nd^{3+} was studied on an electrode previously subjected to Nd^{3+} electrosorption at -89.1 mA g^{-1} for 4 hours. Nd^{3+} release was first tested by immersion in 1 M $KCl_{(aq)}$ for 4 hours at OCP, afterwards the electrode was digested in aqua regia. Analysis of the $KCl_{(aq)}$ solution and digested electrode showed 0.138 mg and 1.67 mg of Nd respectively, which translates to >90% retention of Nd in the electrode. The fact that the majority of the adsorbed Nd was retained in the electrode and not spontaneously released into the KCl solution in the absence of an applied potential strongly suggest that the main adsorption

mechanism is non-capacitive, and an electron transfer reaction was involved. Therefore, electrode polarization at more positive potentials is required to release the Nd^{3+} as shown ahead in the manuscript.

Investigating the Cyclability of the Carbon Electrode —An ideal electrode candidate would show a stable physical and chemical structure and little variability during consecutive cycles of electrosorption and release. The repeatability of the Nd^{3+} electrosorption onto the electrode was investigated over six cycles. Loadings were conducted from 250 mM $NdCl_{3(aq)}$ at -89.1 mA g^{-1} for 4 hours followed by releasing into 1M $KCl_{(aq)}$ at 178 mA g^{-1} for two hours. Fresh $NdCl_{3(aq)}$ and $KCl_{(aq)}$ solutions were employed for each cycle performed. The increase to a more positive release current during desorption (same charge as loading) was employed to investigate the stability of the electrode in aqueous electrolyte. Figure S8a and 7a show that the time vs. potential profiles remain similar during the loading and release cycles. Successive releases into different $KCl_{(aq)}$ electrolytes show an average of 4.19 mg of Nd and a standard deviation of 0.454 as seen in Table S3. Furthermore, as observed in Figure 7b, Nd^{3+} electrosorption shows an increasing trend from cycles 1 to 4 and then tapers off slightly for cycles 5-6. During the release of Nd some binder dissolution (dark brown powder) was observed on the electrolyte as seen in Figure S9. However, the carbon electrode remained visibly intact. This test proves the stability of the electrode material and promising nature of the Vulcan XC-72R for Nd^{3+} capture and release in aqueous solution.

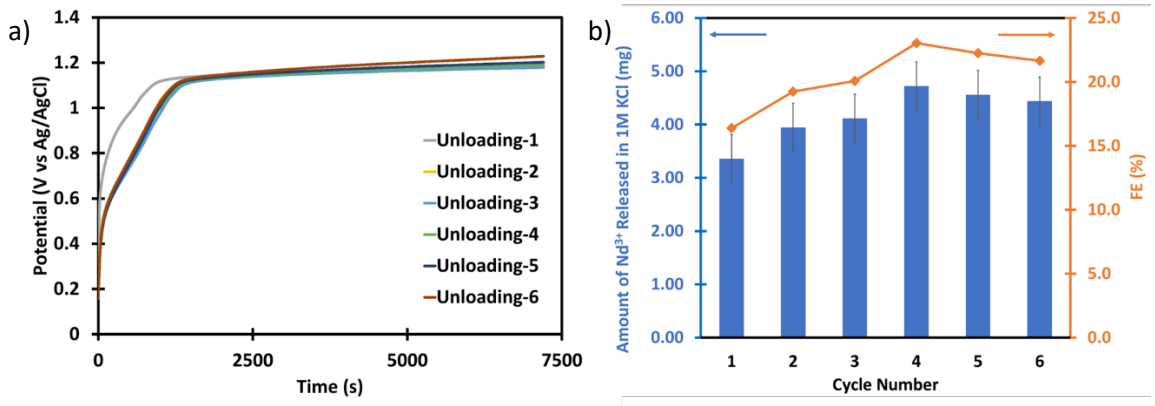

Figure 7. a) Potential time curves for release of Nd into 1 M $KCl_{(aq)}$ at 178 mA g^{-1} b) stability and faradaic efficiency of electrode during cycling, where amount of Nd^{3+} released shows an increasing trend.

Investigating the selective capture of the carbon electrode —To study the selectivity of the carbon electrode towards Na^{+}, Mg^{2+}, and Nd^{3+}, initial experiments were conducted in individual electrolytes containing 250 mM electrolytes of Na^{+}, Mg^{2+}. The current density and duration applied during Na^{+} and Mg^{2+}electrosorption were -89.1 mA g^{-1} and 4 hours respectively. Following loading the release of each ion was done in separate 1 M $KCl_{(aq)}$ solutions. A total of four consecutive loading and release tests were conducted for Na^{+} and Mg^{+} and compared against the Nd^{3+}. The duration of each release was 4 hours at 89.1 mA g^{-1}. Time versus potential curves in Figures 8, S10 and S11 display a similar short lived sloping region, followed by a plateau, suggesting possible electrosorption of Na^{+}, Mg^{2}, Nd^{3+} within pores of the electrode. However, it is interesting to note that the electrosorption plateau for Nd^{3+} during electrolysis is more positive than Mg^{2+} and Na^{+}, following the trend shown by the CV analysis in Figure 2b. The more

positive trend for electrosorption plateau for Nd^{3+} compared to the other cations suggests the possibility of selectivity between the ions.

Furthermore, table S4 shows an average FE of 24.7% for Mg^{2+} electrosorption. This value is comparable to that observed during the electrosorption of Nd^{+}. However, as the charge of the Mg^{2+} ions is lower than that of Nd^{3+}, the average amount of moles of Mg^{2+} captured in the carbon electrode is twice the amount of Nd^{3+}. Also, Figure S11 shows a similar potential profile during the electrosorption of Na^{+} as that observed for Mg^{2+}, and in agreement with the observations made by Cheng et al. for Na^{+} capture in non-aqueous media [15]. However, Table S5 shows that the FE of Na^{+} electrosorption is an order of magnitude lower than that of Mg^{2+} suggesting a possible competition between water/proton electrosorption and Na^{+} [72]. These results motivated the investigation of an electrolyte containing equal concentrations of Nd^{3+}, Mg^{2+}, and Na^{+}.

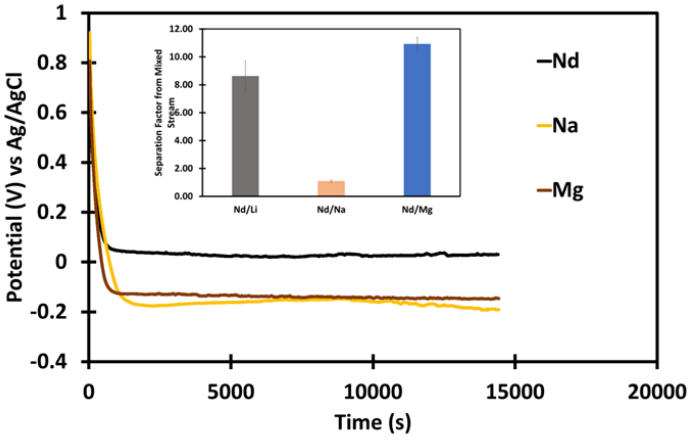

Figure 8. Comparison between potential time curves for Nd^{3+}, Mg^{2+}, and Na^{+} intercalation at -2.85 mA for 4 hours in 250 mM $NdCl_{3\,(aq)}$, $MgCl_{2(aq)}$ and $NaCl_{(aq)}$. Insert: Separation factors between Nd and Li, Na, and Mg in an aqueous electrolyte containing 250 mM each of LiCl, NaCl, $MgCl_2$ and $NdCl_3$

Following investigation of the electrode in electrolytes containing single salts, the selectivity of the carbon electrode towards Nd^{3+} was investigated in an electrolyte containing equimolar concentrations (250mM) of LiCl, KCl, NaCl, $MgCl_2$ and $NdCl_3$. Two successive load-release cycles (into 1 M KCl) were performed with a single electrode at -89.1 mA g^{-1} and 89.1 mA g^{-1} for 4 hours respectively. Comparison between the loading potential time curves of the electrolyte containing all cations, with the electrolytes containing individual cations of Li^{+}, Na^{+}, K^{+} and Mg^{2+} display a more positive plateau for the mixed electrolyte as seen in Figure S12. However, this plateau is only slightly more negative than Nd^{3+} as seen in Figure S12. This observation, which suggests favorability towards Nd^{3+} electrosorption was corroborated by the ICP-MS results displayed in Table S6 where Nd^{3+} correspond to main electrosorbed cations (>50%). Furthermore, the FE for Nd^{3+} capture is significantly larger than the other cations. Zhao et al [8] reported similar findings where trivalent ions were more preferentially adsorbed onto the surface of the electrode. This could in part be due to the strong interactions between the ions and the charged surface [73]. Surprisingly, one would expect Mg^{2+} to be preferentially selected over Li^{+} and Na^{+}, since Mg^{2+} has a higher valence as shown (Table S6) in the single cation electrolytes. However, Na^{+} seems to be preferentially selected in the mixed electrolyte.

A look at the separation factors (SF) based on number moles (Table S6 and inset of Figure 8), shows an average of 8.6 for Nd^{3+}/Li^{+}, and 11.2 for Nd^{3+}/Mg^{2+}. A SF of 1.1 for Nd^{3+}/Na^{+} shows no relevant separation. These results prove selectivity of Nd^{3+} over the other competitive cations with electrosorption capacities up to 125 mg g^{-1}. These values are higher than those reported by Zhao et al. for pure capacitive immobilization of La^{3+} (23.66 mg g^{-1}) [8], and in the same order of magnitude to those reported by Wang et al. for Nd^{3+} and Ce^{3+} (23.66 mg g^{-1}) [9] with the advantage that the pseudocapacive immobilization can be reversed electrochemically to selectively separate and release REE from diluted sources.

Conclusion

Soft and hard carbon materials can be a promising route for REE capture from aqueous stream. This is the first reported study where Nd^{3+} was preferentially electrosorbed from an aqueous stream in the presence of competitive cations employing a Faradaic process where cation capture and release is accompanied by an electron transfer process. The stability of the electrode was tested, and multiple cycling tests showed consistency in Nd^{3+} capture, with excellent cycling.

Potential time curves strongly suggested that electrosorption of cations took place within the pores of the electrode with very little diffusion with interlayer spacings. The very positive time potential curve for Nd^{3+} electrosorption prompted investigation into its selectivity between common competitive cations. Also, increasing duration of electrolysis at a current density of 89.1 mA g^{-1} shows an increase in electrosorption of Nd^{3+}. Furthermore, in the presence of Li^{+}, Na^{+}, K^{+}, and Mg^{+}, Nd^{3+} is selectively electrosorbed, leading to promising separation factors between competitive cations. While this study is still in the preliminary stages of investigation, it does show some promise for REE capture employing soft or hard carbons.

Acknowledgement

This manuscript has been authored by Battelle Energy Alliance, LLC under Contract No. DE-AC07–05ID14517 with the U.S. Department of Energy. This study was supported by funding provided by the Critical Materials Institute, an Energy Innovation Hub funded by the U.S. Department of Energy, Office of Energy Efficiency and Renewable Energy, Advanced Manufacturing Office. The authors wish to also express their sincere thanks to Byron White, and Brittany Tague, from Idaho National Laboratory, for offering their support and expertise during this project.

References

1. Balaram, V., *Rare earth elements: A review of applications, occurrence, exploration, analysis, recycling, and environmental impact.* Geoscience Frontiers, 2019. **10**(4): p. 1285-1303.
2. Engmann, E.T., et al., *Efficient Room Temperature Neodymium Electrodeposition in a Calcium-Based Electrolyte.* ACS Applied Engineering Materials, 2023. **1**(8): p. 2295-2303.
3. Mwewa, B., et al., *Recovery of rare earth elements from acid mine drainage: a review of the extraction methods.* Journal of Environmental Chemical Engineering, 2022. **10**(3): p. 107704.
4. Pan, J., et al., *Recovery of rare earth elements from coal fly ash through sequential chemical roasting, water leaching, and acid leaching processes.* Journal of Cleaner Production, 2021. **284**: p. 124725.
5. Franus, W., M.M. Wiatros-Motyka, and M. Wdowin, *Coal fly ash as a resource for rare earth elements.* Environmental Science and Pollution Research, 2015. **22**: p. 9464-9474.
6. Liu, P., R. Huang, and Y. Tang, *Comprehensive understandings of rare earth element (REE) speciation in coal fly ashes and implication for REE extractability.* Environmental science & technology, 2019. **53**(9): p. 5369-5377.
7. Vapnik, H., J. Elbert, and X. Su, *Redox-copolymers for the recovery of rare earth elements by electrochemically regenerated ion-exchange.* Journal of Materials Chemistry A, 2021. **9**(35): p. 20068-20077.
8. Zhao, F., et al., *Selectively capacitive recovery of rare earth elements from aqueous solution onto Lewis base sites of pyrrolic-N doped activated carbon electrodes.* Carbon, 2022. **197**: p. 282-291.
9. Wang, L., et al., *Recovery of rare earth by electro-sorption with sodium diphenylamine sulfonate modified activated carbon electrode.* Separation and Purification Technology, 2022. **292**: p. 121005.
10. Porada, S., et al., *Review on the science and technology of water desalination by capacitive deionization.* Progress in materials science, 2013. **58**(8): p. 1388-1442.
11. Jiang, Y. and J. Liu, *Definitions of pseudocapacitive materials: a brief review.* Energy & Environmental Materials, 2019. **2**(1): p. 30-37.
12. Mathis, T.S., et al., *Energy storage data reporting in perspective—guidelines for interpreting the performance of electrochemical energy storage systems.* Advanced Energy Materials, 2019. **9**(39): p. 1902007.

13. Liu, Y., S.P. Jiang, and Z. Shao, *Intercalation pseudocapacitance in electrochemical energy storage: recent advances in fundamental understanding and materials development.* Materials Today Advances, 2020. **7**: p. 100072.
14. Cao, Y., et al., *Sodium ion insertion in hollow carbon nanowires for battery applications.* Nano letters, 2012. **12**(7): p. 3783-3787.
15. Cheng, D., et al., *Electrochemical storage mechanism of sodium in carbon materials: A study from soft carbon to hard carbon.* Carbon, 2021. **182**: p. 758-769.
16. Wen, Y., et al., *Expanded graphite as superior anode for sodium-ion batteries.* Nature communications, 2014. **5**(1): p. 4033.
17. Yu, X., et al., *Pseudocapacitance: emergent pseudocapacitance of 2D nanomaterials (Adv. Energy Mater. 13/2018).* Advanced Energy Materials, 2018. **8**(13): p. 1870058.
18. Yoshio, M., R.J. Brodd, and A. Kozawa, *Lithium-ion batteries*. Vol. 1. 2009: Springer.
19. Yang, X., et al., *Surface functional groups of carbon-based adsorbents and their roles in the removal of heavy metals from aqueous solutions: a critical review.* Chemical Engineering Journal, 2019. **366**: p. 608-621.
20. Zukalová, M., et al., *Pseudocapacitive lithium storage in TiO2 (B).* Chemistry of Materials, 2005. **17**(5): p. 1248-1255.
21. Zhu, K., et al., *Pseudocapacitive lithium-ion storage in oriented anatase TiO2 nanotube arrays.* The Journal of Physical Chemistry C, 2012. **116**(22): p. 11895-11899.
22. Cook, J.B., et al., *Mesoporous MoS2 as a transition metal dichalcogenide exhibiting pseudocapacitive Li and Na-ion charge storage.* Advanced Energy Materials, 2016. **6**(9): p. 1501937.
23. Chao, D., et al., *Pseudocapacitive Na-ion storage boosts high rate and areal capacity of self-branched 2D layered metal chalcogenide nanoarrays.* ACS nano, 2016. **10**(11): p. 10211-10219.
24. An, C., et al., *Graphene wrapped FeSe2 nano-microspheres with high pseudocapacitive contribution for enhanced Na-ion storage.* Advanced Energy Materials, 2019. **9**(18): p. 1900356.
25. Liu, Q., et al., *Super long-life potassium-ion batteries based on an antimony@ carbon composite anode.* Chemical communications, 2018. **54**(83): p. 11773-11776.
26. Li, N., F. Zhang, and Y. Tang, *Hierarchical T-Nb 2 O 5 nanostructure*

with hybrid mechanisms of intercalation and pseudocapacitance for potassium storage and high-performance potassium dual-ion batteries. Journal of Materials Chemistry A, 2018. **6**(37): p. 17889-17895.
27. Wang, Y., et al., *Hyperporous sponge interconnected by hierarchical carbon nanotubes as a high-performance potassium-ion battery anode.* Advanced Materials, 2018. **30**(32): p. 1802074.
28. Augustyn, V., P. Simon, and B. Dunn, *Pseudocapacitive oxide materials for high-rate electrochemical energy storage.* Energy & Environmental Science, 2014. **7**(5): p. 1597-1614.
29. Li, Y., et al., *Intercalation chemistry of graphite: alkali metal ions and beyond.* Chemical Society Reviews, 2019. **48**(17): p. 4655-4687.
30. Liu, Y., et al., *Mechanism of lithium insertion in hard carbons prepared by pyrolysis of epoxy resins.* Carbon, 1996. **34**(2): p. 193-200.
31. Stark, M.S., et al., *Intercalation of layered materials from bulk to 2D.* Advanced Materials, 2019. **31**(27): p. 1808213.
32. Luo, W., et al., *Electrochemically expandable soft carbon as anodes for Na-ion batteries.* ACS central science, 2015. **1**(9): p. 516-522.
33. Yao, X., et al., *Defect-rich soft carbon porous nanosheets for fast and high-capacity sodium-ion storage.* Advanced Energy Materials, 2019. **9**(6): p. 1803260.
34. Stevens, D. and J. Dahn, *High capacity anode materials for rechargeable sodium-ion batteries.* Journal of the Electrochemical Society, 2000. **147**(4): p. 1271.
35. Hou, B.H., et al., *Self-supporting, flexible, additive-free, and scalable hard carbon paper self-interwoven by 1D microbelts: superb room/low-temperature sodium storage and working mechanism.* Advanced Materials, 2019. **31**(40): p. 1903125.
36. Choi, J., et al., *Pyroprotein-derived hard carbon fibers exhibiting exceptionally high plateau capacities for sodium ion batteries.* ACS Applied Energy Materials, 2019. **2**(2): p. 1185-1191.
37. Alvin, S., et al., *Revealing sodium ion storage mechanism in hard carbon.* Carbon, 2019. **145**: p. 67-81.
38. Bai, P., et al., *Elucidation of the sodium-storage mechanism in hard carbons.* Advanced Energy Materials, 2018. **8**(15): p. 1703217.
39. Tarascon, J.-M. and M. Armand, *Issues and challenges facing rechargeable lithium batteries.* nature, 2001. **414**(6861): p. 359-367.
40. Piao, T., et al., *Intercalation of lithium ions into graphite electrodes*

studied by AC impedance measurements. Journal of The Electrochemical Society, 1999. **146**(8): p. 2794.
41. Dunn, B., H. Kamath, and J.-M. Tarascon, *Electrical energy storage for the grid: a battery of choices.* Science, 2011. **334**(6058): p. 928-935.
42. Rajagopalan, R., et al., *Advancements and challenges in potassium ion batteries: a comprehensive review.* Advanced Functional Materials, 2020. **30**(12): p. 1909486.
43. Luo, W., et al., *Potassium ion batteries with graphitic materials.* Nano letters, 2015. **15**(11): p. 7671-7677.
44. Rao, K.A. and T. Sreenivas, *Recovery of rare earth elements from coal fly ash: a review.* Critical and rare earth elements: Recovery from secondary resources, 2019: p. 343-364.
45. do Rego, U.A., et al., *Effect of substrate and pyrolysis atmosphere of FeNx materials on electrocatalysis of the oxygen reduction reaction.* Electrocatalysis, 2021. **12**(5): p. 548-563.
46. Short, M. and P. Walker Jr, *Measurement of interlayer spacings and crystal sizes in turbostratic carbons.* Carbon, 1963. **1**(1): p. 3-9.
47. Elton, L. and D.F. Jackson, *X-ray diffraction and the Bragg law.* American Journal of Physics, 1966. **34**(11): p. 1036-1038.
48. Greenberg, B., *Bragg's law with refraction.* Acta Crystallographica Section A: Foundations of Crystallography, 1989. **45**(3): p. 238-241.
49. Lee, H.Y. and J.B. Goodenough, *Supercapacitor behavior with KCl electrolyte.* Journal of Solid State Chemistry, 1999. **144**(1): p. 220-223.
50. Zhang, L.L. and X. Zhao, *Carbon-based materials as supercapacitor electrodes.* Chemical society reviews, 2009. **38**(9): p. 2520-2531.
51. Brousse, T., D. Bélanger, and J.W. Long, *To be or not to be pseudocapacitive?* Journal of The Electrochemical Society, 2015. **162**(5): p. A5185.
52. Pérez-Rodríguez, S., E. Pastor, and M. Lázaro, *Electrochemical behavior of the carbon black Vulcan XC-72R: Influence of the surface chemistry.* International Journal of Hydrogen Energy, 2018. **43**(16): p. 7911-7922.
53. Tang, Y., et al., *Comparative study on three commercial carbons for supercapacitor applications.* Russian Journal of Electrochemistry, 2015. **51**: p. 77-85.
54. Sahu, V., et al., *Synthesis of hydrophilic carbon black; role of hydrophilicity in maintaining the hydration level and protonic conduction.*

RSC advances, 2013. **3**(12): p. 3917-3924.
55. Cao, B., et al., *Mesoporous soft carbon as an anode material for sodium ion batteries with superior rate and cycling performance.* Journal of Materials Chemistry A, 2016. **4**(17): p. 6472-6478.
56. Jian, Z., et al., *Insights on the mechanism of Na-ion storage in soft carbon anode.* Chemistry of Materials, 2017. **29**(5): p. 2314-2320.
57. Medina, A.S., et al., *Electrochemical preconcentration mechanism of trivalent lanthanum.* Journal of The Electrochemical Society, 2018. **165**(13): p. D654.
58. Wang, L., et al., *Ultrahigh-rate and ultralong-life aqueous batteries enabled by special pair-dancing proton transfer.* Science Advances, 2023. **9**(18): p. eadf4589.
59. Zhu, Z., et al., *An ultrafast and ultra-low-temperature hydrogen gas–proton battery.* Journal of the American Chemical Society, 2021. **143**(48): p. 20302-20308.
60. Posada Perez, S., G.-M. Rignanese, and G. Hautier. *Shedding Light about the Role of Proton Intercalation in Layered Cathode Materials By Means of First Principle Computations*. in *Electrochemical Society Meeting Abstracts prime2020*. 2020. The Electrochemical Society, Inc.
61. Wu, X., et al., *Diffusion-free Grotthuss topochemistry for high-rate and long-life proton batteries.* Nature Energy, 2019. **4**(2): p. 123-130.
62. Zhao, Q., et al., *Proton intercalation/de-intercalation dynamics in vanadium oxides for aqueous aluminum electrochemical cells.* Angewandte Chemie International Edition, 2020. **59**(8): p. 3048-3052.
63. Zhou, L., et al., *Opportunities and challenges for aqueous metal-proton batteries.* Matter, 2021. **4**(4): p. 1252-1273.
64. Fares, M.M., F.A.A. Al-Rub, and A.R. Mohammad, *Ultimate eradication of the ciprofloxacin antibiotic from the ecosystem by nanohybrid GO/O-CNTs.* ACS omega, 2020. **5**(9): p. 4457-4468.
65. Ortiz, S.N.C., R. Cabanzo, and E. Mejia-Ospino, *Crude oil/water emulsion separation using graphene oxide and amine-modified graphene oxide particles.* Fuel, 2019. **240**: p. 162-168.
66. Zheng, T., J. Reimers, and J. Dahn, *Effect of turbostratic disorder in graphitic carbon hosts on the intercalation of lithium.* Physical Review B, 1995. **51**(2): p. 734.
67. Ru, H., et al., *Bean-dreg-derived carbon materials used as superior anode material for lithium-ion batteries.* Electrochimica acta, 2016. **222**: p.

551-560.
68. Alcorn, F.M., et al., *Aqueous Intercalation of Graphite at a Near-Neutral pH.* ACS Applied Energy Materials, 2018. **1**(9): p. 5062-5067.
69. Khan, A., *Installation and operation of autosorb-1-C-8 for bet surface area measurement of porous materials*. 2010, Pakistan Institute of Nuclear Science and Technology.
70. Carmo, M., et al., *Physical and electrochemical evaluation of commercial carbon black as electrocatalysts supports for DMFC applications.* Journal of Power Sources, 2007. **173**(2): p. 860-866.
71. Narten, A. and R. Hahn, *Hydration of the neodymium (3+) ion in neodymium chloride solutions determined by neutron diffraction.* The Journal of Physical Chemistry, 1983. **87**(17): p. 3193-3197.
72. Zhang, X., et al., *Revealing the Competitive Intercalation between Na+ and H+ into Na0. 44MnO2 in Aqueous Sodium Ion Batteries.* Advanced Energy Materials, 2023. **13**(17): p. 2204413.
73. Chen, R., et al., *Capacitive deionization and electrosorption for heavy metal removal.* Environmental Science: Water Research & Technology, 2020. **6**(2): p. 258-282.